

# FISTA ITERATES CONVERGE LINEARLY FOR DENOISER-DRIVEN REGULARIZATION\*

ARGHYA SINHA<sup>†</sup> AND KUNAL N. CHAUDHURY<sup>‡</sup>

**Abstract.** The effectiveness of denoising-driven regularization for image reconstruction has been widely recognized. Two prominent algorithms in this area are Plug-and-Play (PnP) and Regularization-by-Denoising (RED). We consider two specific algorithms PnP-FISTA and RED-APG, where regularization is performed by replacing the proximal operator in the FISTA algorithm with a powerful denoiser. The iterate convergence of FISTA is known to be challenging with no universal guarantees. Yet, we show that for linear inverse problems and a class of linear denoisers, global linear convergence of the iterates of PnP-FISTA and RED-APG can be established through simple spectral analysis.

**Key words.** image regularization, plug-and-play, regularization-by-denoising, FISTA, linear convergence.

**MSC codes.** 94A08, 41A25, 65F10

**1. Introduction.** Over the past decade, there has been a growing interest in applying denoisers for iterative reconstruction. This trend was triggered by the seminal works [31, 34], where the idea of using off-the-shelf denoisers for regularization was formalized. Subsequent studies have revealed that trained denoisers produce results that are competitive with end-to-end deep learning methods. Notably, this approach allows us to combine robust denoising priors with model-based inversion for variational regularization.

The effectiveness of denoiser-driven regularization has motivated researchers to investigate its convergence properties [8, 10, 12, 14, 15, 18, 20, 26, 29, 30, 32, 37]. We refer the reader to the recent article [9] for an excellent survey on denoiser-driven regularization. The convergence theory in this area is primarily motivated by convex optimization and monotone operator theory [2, 33]. Indeed, a common theme in many of these papers is to guarantee convergence by designing an appropriate regularizer [8, 18] or by restricting the denoiser (during training or by design) to a class of nonexpansive operators [16, 29]. While the current focus is on trained denoisers, it is also known that their black-box nature can lead to unpredictable behavior; e.g., see Figure 1, [26, Fig. 6], and [36, Fig. 1]. Moreover, the convergence guarantees for these denoisers are often based on assumptions that are difficult to verify in practice. In this work, we demonstrate that using a class of data-driven linear denoisers, which are not state-of-the-art but still give good reconstructions [25, 27, 34], we can get strong convergence guarantees under fully verifiable assumptions.

**1.1. PnP and RED.** We consider two popular regularization methods, Plug-and-Play (PnP) and Regularization-by-Denoising (RED). In particular, we revisit the PnP-FISTA and RED-APG (RED-Accelerated Proximal Gradient) algorithms [10, 30] that are modeled on the classical FISTA algorithm (Fast Iterative-Shrinkage Thresholding Algorithm). This is an accelerated first-order method for solving convex optimization problems of the form

$$(1.1) \quad \min_{\mathbf{x} \in \mathbb{R}^n} f(\mathbf{x}) + g(\mathbf{x}),$$

where  $f$  is smooth and  $g$  is nonsmooth but proximable [4]. In image reconstruction,  $f$  is a model-based loss function, and  $g$  is an image regularizer. Starting with an initialization

\* **Funding:** A. Sinha was supported by PMRF Fellowship TF/PMRF-22-5534 and K. N. Chaudhury was supported by grants CRG/2020/000527 and STR/2021/000011 from the Government of India.

<sup>†</sup>Department of Computational and Data Sciences, Indian Institute of Science, Bangalore (arghyasinha@iisc.ac.in).

<sup>‡</sup>Department of Electrical Engineering, Indian Institute of Science, Bangalore (kunal@iisc.ac.in).

$\mathbf{y}_1 = \mathbf{x}_0$  and  $t_1 = 1$ , FISTA generates a sequence of images  $\{\mathbf{x}_k\}_{k \geq 1}$  using the updates:

$$(1.2a) \quad \mathbf{x}_k = \text{prox}_{\gamma g}(\mathbf{y}_k - \gamma \nabla f(\mathbf{y}_k)),$$

$$(1.2b) \quad t_{k+1} = \frac{1}{2} \left( 1 + \sqrt{1 + 4t_k^2} \right),$$

$$(1.2c) \quad \mathbf{y}_{k+1} = \mathbf{x}_k + \frac{t_k - 1}{t_{k+1}} (\mathbf{x}_k - \mathbf{x}_{k-1}),$$

where  $\text{prox}_{\gamma g}$  is the proximal operator of  $\gamma g$  and  $\gamma > 0$  is the step size. For sufficiently small  $\gamma$  and appropriate technical assumptions on  $f$  and  $g$ , it was shown by Beck and Teboulle that the objective  $f(\mathbf{x}_k) + g(\mathbf{x}_k)$  converges sublinearly to the minimum of (1.1).

In PnP-FISTA, the proximal operator (which effectively performs image denoising) is substituted by a powerful denoiser, i.e., the update in (1.2a) is performed as

$$(1.3) \quad \mathbf{x}_k = \mathbf{W}(\mathbf{y}_k - \gamma \nabla f(\mathbf{y}_k)),$$

where  $\mathbf{W}$  is a denoising operator. In this note, we will work with a particular class of linear denoisers. This includes kernel denoisers such as NLM [6, 34], LARK, and GLIDE [23]. This is the simplest PnP model that works well in practice [10, 11, 34] and yet is analytically tractable. We wish to emphasize that this class of denoisers is not strictly “linear” like the simple Gaussian or the box filter. Rather, the action of the denoiser is given by  $\mathbf{x} \mapsto \mathbf{W}(\mathbf{x}_g) \mathbf{x}$  which acts linearly on the input image  $\mathbf{x}$  and depends non-linearly on a guide image  $\mathbf{x}_g$ ; the latter serves as a surrogate for the ground truth image. In fact, it is precisely this data-driven nature, referred to as “pseudo-linearity” [22], that makes them more effective than classical linear denoisers. In iterative image reconstruction, the initial guide image serves as a rough estimate that evolves over the first few iterations as per the updates in (1.3). To achieve high-quality reconstructions [10, 34], a common practice is to fix the guide image after a certain number of iterations. Thus, as far as the question of convergence is concerned, we can assume the denoiser to be a purely linear operator  $\mathbf{x} \mapsto \mathbf{W}\mathbf{x}$ . While the choice of guide determines the reconstruction quality, it has no direct bearing on the convergence problem.

In PnP-FISTA, we treat the loss  $f$  as the smooth component of the objective function. On the other hand, in RED-APG, the accelerated variant of RED, we work with the first-order approximation of the regularizer  $g$  [30, Sec. V]. More precisely, starting with  $t_0 = 1$  and  $\mathbf{v}_0 \in \mathbb{R}^n$ , the updates in RED-APG are given by

$$(1.4a) \quad \mathbf{x}_k = \text{prox}_{(\lambda L)^{-1} f}(\mathbf{v}_{k-1}),$$

$$(1.4b) \quad t_k = \frac{1}{2} \left( 1 + \sqrt{1 + 4t_{k-1}^2} \right),$$

$$(1.4c) \quad \mathbf{y}_k = \mathbf{x}_k + \frac{t_{k-1} - 1}{t_k} (\mathbf{x}_k - \mathbf{x}_{k-1}),$$

$$(1.4d) \quad \mathbf{v}_k = \theta \mathbf{W}(\mathbf{y}_k) + (1 - \theta) \mathbf{y}_k,$$

where  $\lambda > 0$ ,  $L \geq 1$  are the internal parameters and  $\theta = 1/L$ .

**1.2. Relation to prior work.** Although PnP was originally conceived from an algorithmic point-of-view, the iterations in PnP-FISTA can nonetheless be seen as solving an optimization problem of the form (1.1). As a result, we can establish objective convergence of PnP-FISTA and RED-APG using existing results [3, 4]. In this work, we analyze their iterate convergence. This was motivated by a recent work [1], where we were able to establish global linear convergence of PnP-ISTA, which is modeled on the ISTA algorithm for minimizing (1.1). It is known that FISTA is faster than its non-accelerated counterpart ISTA in terms of objective convergence [4]; however, there is no direct relation in terms of iterate convergence (see Figure 5). In fact, while we can guarantee iterate convergence of ISTA using the concept of Mann iterations [3], establishing iterate convergence of FISTA is challenging with no universal convergence guarantees. In this direction, Chambolle

and Dossal [7] have shown that a different choice of momentum parameters can guarantee iterate convergence. Lorenz and Pock obtained similar results [21], although neither work established the convergence rate. On the other hand, asymptotic linear convergence of FISTA was established by Tao et al. [35] and Johnstone and Moulin [19] for sparse minimization such as LASSO. Similar to our work, spectral analysis of the underlying operators comes up in [35]; however, their overall analysis is much more intricate due to the nonlinearity of the denoising operator in LASSO. Notably, the results mentioned above do not apply to PnP-FISTA and RED-APG. In fact, to the best of our knowledge, convergence analysis of these algorithms has not been reported in the literature.

The present contribution lies in establishing global linear convergence of the PnP-FISTA and RED-APG iterates in the context of linear inverse problems and data-driven linear denoisers. In this regard, we wish to comment on prior convergence results for linear denoisers [10, 12, 20, 34]. In [10, 34], it was demonstrated that PnP with kernel denoisers can be formulated as a convex optimization problem of the form (1.1); objective convergence of PnP-FISTA and PnP-ADMM was subsequently established using standard optimization theory. Iterate convergence of PnP-ISTA and PnP-ADMM (but not PnP-FISTA) follows from standard results [2]. However, since the smooth part  $f$  in (1.1) is typically not strongly convex, it is non-trivial to establish linear convergence. Yet, it was shown in [12, 20] that linear convergence can be established for PnP-ISTA. However, the analysis in these papers is tailored to the inpainting problem and relies on assumptions that are difficult to interpret and validate. More recently, we developed a convergence theory for PnP-ISTA and PnP-ADMM in [1] based on practically verifiable assumptions. A key difference with [1] is that we work with the spectral radius instead of controlling a specific norm.

**1.3. Notations.** We use  $\mathbf{0}$  and  $\mathbf{1}$  to denote the all-zeros and the all-ones vectors in  $\mathbb{R}^n$ , the dimension  $n$  should be clear from the context. We use  $\mathbf{0}_n$  and  $\mathbf{I}_n$  for the zero and identity operators on  $\mathbb{R}^n$ . The space of symmetric linear operators on  $\mathbb{R}^n$  is denoted by  $\mathbb{S}^n$ . We use  $\text{fix}(\mathbf{W})$  for the fixed points of  $\mathbf{W}$ ,  $\ker(\mathbf{A})$  for the kernel of  $\mathbf{A}$ ,  $\sigma(\mathbf{B})$  and  $\rho(\mathbf{B})$  for the spectrum and the spectral radius of  $\mathbf{B}$ ,  $\text{diag}(\mathbf{u})$  for the diagonal matrix with  $\mathbf{u}$  as the diagonal elements,  $\mathbf{A} \sim \mathbf{B}$  to mean that  $\mathbf{A}$  and  $\mathbf{B}$  are similar,  $\text{span}(\mathbf{u})$  for the space spanned by vector  $\mathbf{u}$ , and  $\|\cdot\|_1$ ,  $\|\cdot\|_2$  and  $\|\cdot\|_\infty$  to denote the  $\ell_1$ ,  $\ell_2$  and  $\ell_\infty$  norms. A matrix  $\mathbf{W}$  is said to be stochastic if  $\mathbf{W}$  is nonnegative and each of its rows sum to 1. In addition,  $\mathbf{W}$  is said to be irreducible if the directed graph associated with  $\mathbf{W}$  is strongly connected [17].

**1.4. Organization.** We discuss kernel denoisers and the forward model in Section 2, the main results are derived in Section 3, and we give numerical simulations in Section 4.

**2. Background.** We consider the problem of recovering an unknown image  $\xi \in \mathbb{R}^n$  from linear measurements  $\mathbf{b} = \mathbf{A}\xi + \mathbf{e}$ , where  $\mathbf{A} \in \mathbb{R}^{m \times n}$  is the forward operator,  $\mathbf{b} \in \mathbb{R}^m$  is the observed image, and  $\mathbf{e} \in \mathbb{R}^m$  is white Gaussian noise. In particular, we will use the standard loss function

$$(2.1) \quad f(\mathbf{x}) = \frac{1}{2} \|\mathbf{A}\mathbf{x} - \mathbf{b}\|_2^2.$$

As mentioned earlier, we will abstractly work with a linear denoiser  $\mathbf{W} \in \mathbb{R}^{n \times n}$  that transforms a noisy image  $\mathbf{x}$  into  $\mathbf{W}\mathbf{x}$ , where  $\mathbf{x}$  is a vectorized representation of the image and  $n$  is the number of pixels. We will initially perform the analysis for a symmetric  $\mathbf{W}$ . Later, in Subsection 3.3, we will extend the results to nonsymmetric denoisers. We do not require the precise definition of  $\mathbf{W}$  but rather consider the following property.

ASSUMPTION 2.1.  $\sigma(\mathbf{W}) \subset [0, 1]$  and  $\ker(\mathbf{A}) \cap \text{fix}(\mathbf{W}) = \{\mathbf{0}\}$ .

We will subsequently show that the above assumption holds for a specific class of denoisers called kernel denoisers [22], which includes NLM [6] and its symmetric variants [23, 34]. Broadly speaking, a kernel denoiser is obtained by considering a kernel function and using it to measure the affinity between pairs of pixels. This gives us a kernel operator  $\mathbf{K} \in \mathbb{R}^{n \times n}$ , where  $\mathbf{K}_{ij}$  encodes the affinity between pixels  $i$  and  $j$ . As mentioned earlier,  $\mathbf{K}$

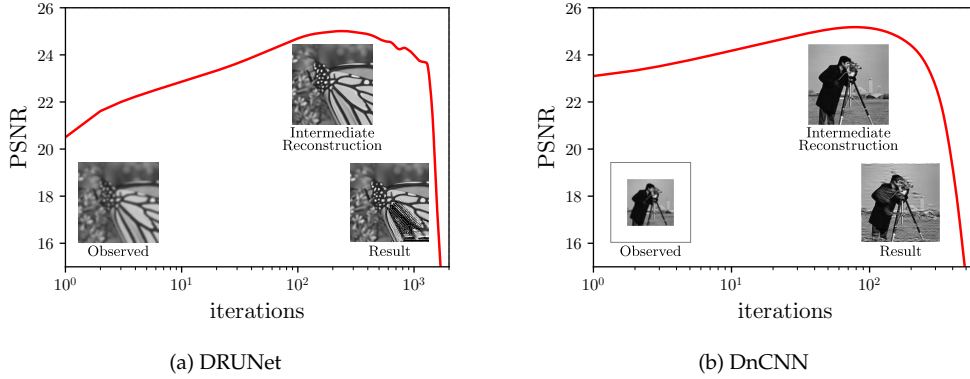


FIG. 1. An example demonstrating the divergence of PnP-ISTA with two commonly used deep denoisers, DRUNet [38] and DnCNN [39]. The result in (a) is for Gaussian deblurring ( $9 \times 9$  kernel with a standard deviation of 4), and that in (b) for superresolution ( $25 \times 25$  Gaussian blur with a standard deviation of 1.6 and  $2 \times$  downsampling). In both examples, we observe that the PSNR initially improves but then declines after a certain point as the iterates diverge. Similar results have been reported in [36].

is computed from a surrogate of the ground truth, called the guide image. More specifically, the kernel in NLM has the form

$$(2.2) \quad \mathbf{K}_{ij} = \varphi(\zeta(i) - \zeta(j)) h(i - j),$$

where  $\varphi$  is a multivariate Gaussian,  $\zeta(i)$  is a patch around pixel  $i$  extracted from the guide image, and  $h$  is a symmetric box or hat function supported on a window around the origin. The denoiser is obtained by normalizing  $\mathbf{K}$ :

$$(2.3) \quad \mathbf{W}_{\text{NLM}} = \mathbf{D}^{-1} \mathbf{K}, \quad \mathbf{D} := \text{diag}(\mathbf{K} \mathbf{1}).$$

It is evident that (2.3) need not be symmetric. We can construct a symmetric variant of (2.3) using the protocol for DSG-NLM [34]:

$$(2.4) \quad \mathbf{W}_{\text{SYM}} = \frac{1}{\|\hat{\mathbf{1}}\|_{\infty}} \mathbf{D}^{-\frac{1}{2}} \mathbf{K} \mathbf{D}^{-\frac{1}{2}} + \text{diag} \left( \mathbf{1} - \frac{1}{\|\hat{\mathbf{1}}\|_{\infty}} \hat{\mathbf{1}} \right), \quad \hat{\mathbf{1}} := \mathbf{D}^{-\frac{1}{2}} \mathbf{K} \mathbf{D}^{-\frac{1}{2}} \mathbf{1},$$

where we use the subscript SYM to distinguish it from (2.3). We refer the reader to [22] for more details on such denoisers.

Kernel denoisers come with a rich set of mathematical properties. We abstract out the specific properties required for our analysis.

**PROPOSITION 2.2.** *Suppose  $\mathbf{K}$  is symmetric positive semidefinite, irreducible, and nonnegative with  $\mathbf{K}_{ii} > 0$  for  $1 \leq i \leq n$ . Then (2.3) and (2.4) are well-defined, stochastic, and irreducible, and their eigenvalues are in  $[0, 1]$ .*

In particular, (2.2) satisfies the assumptions in Proposition 2.2. The details can be found in [34, Sec. IV], which also has the proof of the assertions in Proposition 2.2.

We next verify Assumption 2.1 for denoisers (2.3) and (2.4), when  $\mathbf{A}$  corresponds to inpainting, deblurring, or superresolution. We assume that at least one pixel is sampled for inpainting, and the lowpass blur is nonnegative (and nonzero) for deblurring and superresolution; these technical conditions are typically met in practice [5].

**PROPOSITION 2.3.** *Suppose  $\mathbf{W}$  is (2.3) or (2.4), and the forward operator  $\mathbf{A}$  corresponds to inpainting, deblurring, or superresolution. Then Assumption 2.1 holds.*

*Proof.* From Proposition 2.2, we have  $\rho(\mathbf{W}_{\text{NLM}}) = 1$  and  $\mathbf{1} \in \text{fix}(\mathbf{W}_{\text{NLM}})$ . Moreover, since  $\mathbf{W}_{\text{NLM}}$  is irreducible, we can conclude from the Perron-Frobenius theorem [17] that

$\text{fix}(\mathbf{W}_{\text{NLM}}) = \text{span}(\mathbf{1})$ . Thus, we are done if we can show that  $\mathbf{A}\mathbf{1} \neq \mathbf{0}$ . Indeed, it is clear that  $\mathbf{A}\mathbf{1} \neq \mathbf{0}$  for inpainting and deblurring. Moreover, since  $\mathbf{A}$  is a lowpass blur followed by downsampling in superresolution, we cannot have  $\mathbf{A}\mathbf{1} = \mathbf{0}$ . A similar argument also goes for  $\mathbf{W}_{\text{SYM}}$ .  $\square$

**3. Convergence Analysis.** It was noted in prior works that we can establish convergence of FISTA for different step size rules [7, 21]. This is also the case for PnP-FISTA and RED-APG. In particular, instead of PnP-FISTA, we will work with Algorithm 3.1, where we have replaced the momentum parameter  $(t_k - 1)/t_{k+1}$  in (1.2b) by  $\alpha_k$ . Similarly, instead of RED-APG, we will work with Algorithm 3.2.

---

**Algorithm 3.1**  $\alpha$ -PnP-FISTA

---

- 1: **input:** loss  $f$ , denoiser  $\mathbf{W}$ ,  $\mathbf{x}_0$ ,  $\{\alpha_k\}_{k \geq 1}$  and  $\lambda > 0$ ,  $\gamma > 0$ .
  - 2: **set:**  $\mathbf{y}_1 = \mathbf{x}_0$ .
  - 3: **for**  $k \geq 1$  **do**
  - 4:    $\mathbf{x}_k = \mathbf{W}(\mathbf{y}_k - \gamma \nabla f(\mathbf{y}_k))$ .
  - 5:    $\mathbf{y}_{k+1} = \mathbf{x}_k + \alpha_k (\mathbf{x}_k - \mathbf{x}_{k-1})$ .
  - 6: **end for**
- 

---

**Algorithm 3.2**  $\alpha$ -RED-APG

---

- 1: **input:** loss  $f$ , denoiser  $\mathbf{W}$ ,  $\mathbf{v}_0$ ,  $\{\alpha_k\}_{k \geq 1}$  and  $\lambda > 0$ ,  $L \geq 1$ .
  - 2: **set:**  $\theta = 1/L$ .
  - 3: **for**  $k \geq 1$  **do**
  - 4:    $\mathbf{x}_k = \text{prox}_{(\lambda L)^{-1} f}(\mathbf{v}_{k-1})$ .
  - 5:    $\mathbf{y}_k = \mathbf{x}_k + \alpha_k (\mathbf{x}_k - \mathbf{x}_{k-1})$ .
  - 6:    $\mathbf{v}_k = \theta \mathbf{W}(\mathbf{y}_k) + (1 - \theta) \mathbf{y}_k$ .
  - 7: **end for**
- 

We will analyze the iterate convergence of Algorithm 3.1 and Algorithm 3.2. The key idea is to express the evolution of the iterates as a linear dynamical system in higher dimensions.

**3.1. Preliminaries.** We say that a sequence  $\{\mathbf{x}_k\} \subset \mathbb{R}^n$  converges linearly to  $\mathbf{x}^* \in \mathbb{R}^n$  if there exists a norm  $\|\cdot\|$  on  $\mathbb{R}^n$ ,  $K \geq 1$ ,  $C > 0$ , and  $\beta \in [0, 1)$  such that  $\|\mathbf{x}_k - \mathbf{x}^*\| \leq C\beta^k$  for all  $k \geq K$ . This asymptotic form of convergence is called “local” linear convergence in [19, 35]. However, since we use the term “global convergence” to mean that the sequence converges for any initialization, we will not use “local” and refer to this as linear convergence. The notion of linear convergence does not depend on the choice of norm.

We make the following elementary observation regarding the convergence of a time-varying linear dynamical system.

**LEMMA 3.1.** *Suppose we are given  $\mathbf{s} \in \mathbb{R}^d$  and a sequence of linear operators  $\{\mathbf{R}_k\}_{k \geq 1} \subset \mathbb{R}^{d \times d}$ . For all  $k \geq 1$ , define the affine map  $\mathbf{T}_k : \mathbb{R}^d \rightarrow \mathbb{R}^d$ ,  $\mathbf{T}_k(\mathbf{z}) = \mathbf{R}_k \mathbf{z} + \mathbf{s}$ . Suppose there exists  $\mathbf{R}_\infty \in \mathbb{R}^{d \times d}$  such that*

1.  $\rho(\mathbf{R}_\infty) < 1$ ,
2.  $\lim_{k \rightarrow \infty} \mathbf{R}_k = \mathbf{R}_\infty$ , and
3.  $\bigcap_{k=1}^{\infty} \text{fix}(\mathbf{T}_k) \neq \emptyset$ .

*Then there exists a unique  $\mathbf{z}^* \in \mathbb{R}^d$  such that, for any  $\mathbf{z}_0 \in \mathbb{R}^d$ , the sequence  $\{\mathbf{z}_k\}_{k \geq 0}$  generated via  $\mathbf{z}_{k+1} = \mathbf{T}_k(\mathbf{z}_k)$  converges linearly to  $\mathbf{z}^*$ .*

*Proof.* Fix  $\beta < 1$  such that  $\rho(\mathbf{R}_\infty) < \beta$ . By [17, Lemma 5.6.10], there exists a nonsingular matrix  $\mathbf{Q} \in \mathbb{R}^{d \times d}$  such that, if we define the norm  $\|\mathbf{x}\|_\beta := \|\mathbf{Q}\mathbf{x}\|_1$  on  $\mathbb{R}^d$ , then

$$\rho(\mathbf{R}_\infty) \leq \|\mathbf{R}_\infty\|_\beta < \beta,$$

where  $\|\cdot\|_\beta$  is the operator norm induced by  $\|\cdot\|_\beta$ .

Now, since  $\|\mathbf{R}_k - \mathbf{R}_\infty\|_\beta \rightarrow 0$ , we can find  $K \geq 1$  such that  $\|\mathbf{R}_k\|_\beta \leq \beta$  for all  $k \geq K$ .

Let  $\mathbf{z}^* \in \bigcap_{k=1}^\infty \text{fix}(\mathbf{T}_k)$ , i.e.,  $\mathbf{z}^* = \mathbf{T}_k(\mathbf{z}^*)$  for all  $k \geq 1$ . We can write

$$\mathbf{z}_{k+1} - \mathbf{z}^* = \mathbf{T}_k(\mathbf{z}_k) - \mathbf{T}_k(\mathbf{z}^*) = \mathbf{R}_k(\mathbf{z}_k - \mathbf{z}^*).$$

Hence, for all  $k \geq K$ , we have

$$\|\mathbf{z}_{k+1} - \mathbf{z}^*\|_\beta \leq \|\mathbf{R}_k\|_\beta \|\mathbf{z}_k - \mathbf{z}^*\|_\beta \leq \beta \|\mathbf{z}_k - \mathbf{z}^*\|_\beta.$$

Iterating this, we get

$$\forall k \geq K : \quad \|\mathbf{z}_{k+1} - \mathbf{z}^*\|_\beta \leq \|\mathbf{z}_K - \mathbf{z}^*\|_\beta \cdot \beta^{k+1-K} = C\beta^{k+1},$$

where  $C$  does not depend on  $k$ . Thus, we have shown that  $\{\mathbf{z}_k\}$  converges linearly to  $\mathbf{z}^*$  for any initialization  $\mathbf{z}_0$ .

Finally, note that  $\bigcap_{k=1}^\infty \text{fix}(\mathbf{T}_k)$  must be a singleton. This is because  $\mathbf{z}^* = \mathbf{R}_k \mathbf{z}^* + \mathbf{s}$  for all  $k \geq 1$ . Consequently, letting  $k \rightarrow \infty$ , we get

$$(3.1) \quad (\mathbf{I}_d - \mathbf{R}_\infty) \mathbf{z}^* = \mathbf{s}$$

As  $\rho(\mathbf{R}_\infty) < 1$ ,  $\mathbf{I}_d - \mathbf{R}_\infty$  is nonsingular, and hence (3.1) has at most one solution.  $\square$

We record a result that is required later in the analysis.

PROPOSITION 3.2. *Let  $\mathbf{P} \in \mathbb{R}^{n \times n}$  be such that  $\sigma(\mathbf{P}) \subset [0, 1)$ . If  $\mathbf{R} \in \mathbb{R}^{2n \times 2n}$  is defined to be*

$$\mathbf{R} = \begin{pmatrix} 2\mathbf{P} & -\mathbf{P} \\ \mathbf{I}_n & \mathbf{0}_n \end{pmatrix},$$

then  $\rho(\mathbf{R}) < 1$ .

*Proof.* Let  $\lambda \in \mathbb{C}$  be a nonzero eigenvalue of  $\mathbf{R}$ . By definition, there exists  $\mathbf{z}_1, \mathbf{z}_2 \in \mathbb{R}^n$  such that  $(\mathbf{z}_1, \mathbf{z}_2) \neq \mathbf{0}$ , and

$$(3.2a) \quad 2\mathbf{P}\mathbf{z}_1 - \mathbf{P}\mathbf{z}_2 = \lambda\mathbf{z}_1,$$

$$(3.2b) \quad \mathbf{z}_1 = \lambda\mathbf{z}_2.$$

We claim that  $\lambda \neq 1/2$  and  $\mathbf{z}_1 = \mathbf{0}$ . Indeed, if  $\lambda = 1/2$ , we would obtain  $\mathbf{z}_1 = \mathbf{z}_2 = \mathbf{0}$ , contrary to our assumption. Similarly,  $\mathbf{z}_1 = \mathbf{0}$  would imply (as  $\lambda \neq 0$ ) that  $\mathbf{z} = \mathbf{0}$ .

Substituting (3.2b) in (3.2a), we have

$$(3.3) \quad \mathbf{P}\mathbf{z}_1 = \mu\mathbf{z}_1, \quad \mu := \frac{\lambda^2}{2\lambda - 1}.$$

Since  $\mathbf{z}_1 \neq \mathbf{0}$ , it follows from (3.3) that  $\mu \in \sigma(\mathbf{P})$ . Moreover, we have

$$\lambda^2 - 2\mu\lambda + \mu = 0.$$

As  $\mu \in [0, 1)$  by assumption, we have  $\lambda = \mu \pm i\sqrt{\mu - \mu^2}$ . In either case,  $|\lambda| = \sqrt{\mu} < 1$ .  $\square$

We next prove a result about the spectrum of a particular operator involving the forward model  $\mathbf{A}$  and the denoising operator  $\mathbf{W}$ .

LEMMA 3.3. *For  $\mathbf{W} \in \mathbb{S}^n$  and  $\mathbf{A} \in \mathbb{R}^{m \times n}$  satisfying Assumption 2.1, define*

$$(3.4) \quad \mathbf{P}_\gamma = \mathbf{W}(\mathbf{I}_n - \gamma\mathbf{A}^\top\mathbf{A}) \quad \text{and} \quad \mathbf{P}_{\mu,\theta} = (\mathbf{I}_n + \mu\mathbf{A}^\top\mathbf{A})^{-1}(\theta\mathbf{W} + (1-\theta)\mathbf{I}).$$

Then  $\sigma(\mathbf{P}_\gamma) \subset [0, 1)$  for all  $\gamma \in (0, 1/\lambda_{\max}(\mathbf{A}^\top\mathbf{A}))$  and  $\sigma(\mathbf{P}_{\mu,\theta}) \subset [0, 1)$  for all  $\theta \in [0, 1]$ ,  $\mu > 0$ .

We need the following observation to prove Lemma 3.3.

PROPOSITION 3.4. *Let  $\mathbf{M} \in \mathbb{S}^n$  and  $\sigma(\mathbf{M}) \subset [0, 1]$ . Then  $\|\mathbf{M}\mathbf{x}\| = \|\mathbf{x}\|$  if and only if  $\mathbf{M}\mathbf{x} = \mathbf{x}$ .*

*Proof of Lemma 3.3.* Defining  $\mathbf{G}_\gamma = \mathbf{I}_n - \gamma\mathbf{A}^\top\mathbf{A} \in \mathbb{S}^n$  we have that  $\sigma(\mathbf{G}_\gamma) \subset (0, 1]$  for  $0 < \gamma < 1/\lambda_{\max}(\mathbf{A}^\top\mathbf{A})$ . In particular, as  $\mathbf{G}_\gamma$  is nonsingular, we can write

$$\mathbf{P}_\gamma = \mathbf{G}_\gamma^{-\frac{1}{2}} \left( \mathbf{G}_\gamma^{\frac{1}{2}} \mathbf{W} \mathbf{G}_\gamma^{\frac{1}{2}} \right) \mathbf{G}_\gamma^{\frac{1}{2}} \sim \mathbf{G}_\gamma^{\frac{1}{2}} \mathbf{W} \mathbf{G}_\gamma^{\frac{1}{2}}.$$

Thus, we have  $\sigma(\mathbf{P}_\gamma) \subset [0, \infty)$  since  $\mathbf{W}$  is positive semidefinite. Using Proposition 3.4, we will establish the stronger result that  $\rho(\mathbf{P}_\gamma) < 1$ . In fact, we know that<sup>1</sup>

$$\rho(\mathbf{P}_\gamma) \leq \max_{\|\mathbf{x}\|_2=1} \|\mathbf{P}_\gamma\mathbf{x}\|_2.$$

Thus, it suffices to show that  $\|\mathbf{P}_\gamma\mathbf{x}\|_2 < 1$  for all  $\|\mathbf{x}\|_2 = 1$ .

Note that  $\|\mathbf{W}\|_2 \leq 1$  and  $\|\mathbf{G}_\gamma\|_2 \leq 1$ . Let  $\mathbf{x} \in \mathbb{R}^n$  such that  $\|\mathbf{x}\|_2 = 1$ . We have two possibilities: (i)  $\mathbf{x} \in \ker(\mathbf{A})$ , and (ii)  $\mathbf{x} \notin \ker(\mathbf{A})$ . For (i), we must have  $\mathbf{x} \notin \text{fix}(\mathbf{W})$ , since  $\ker(\mathbf{A}) \cap \text{fix}(\mathbf{W}) = \{\mathbf{0}\}$ . Hence, from Proposition 3.4, we get  $\|\mathbf{W}\mathbf{x}\|_2 < \|\mathbf{x}\|_2$ . Moreover, since  $\mathbf{G}_\gamma\mathbf{x} = \mathbf{x}$ ,

$$\|\mathbf{P}_\gamma\mathbf{x}\|_2 = \|\mathbf{W}(\mathbf{G}_\gamma\mathbf{x})\|_2 \leq \|\mathbf{W}\mathbf{x}\|_2 < \|\mathbf{x}\|_2.$$

For (ii), we have  $\mathbf{G}_\gamma\mathbf{x} \neq \mathbf{x}$ ; hence  $\|\mathbf{G}_\gamma\mathbf{x}\|_2 < \|\mathbf{x}\|_2$  by Proposition 3.4. Again,

$$\|\mathbf{P}_\gamma\mathbf{x}\|_2 = \|\mathbf{W}(\mathbf{G}_\gamma\mathbf{x})\|_2 \leq \|\mathbf{G}_\gamma\mathbf{x}\|_2 < \|\mathbf{x}\|_2.$$

Thus, we have shown that  $\sigma(\mathbf{P}_\gamma) \subset [0, 1)$ .

The other result  $\sigma(\mathbf{P}_{\mu,\theta}) \subset [0, 1)$  follows similarly. In particular, we can write  $\mathbf{P}_{\mu,\theta} = \mathbf{H}\mathbf{W}_\theta$ , where  $\mathbf{H} := (\mathbf{I} + \mu\mathbf{A}^\top\mathbf{A})^{-1}$  and  $\mathbf{W}_\theta := \theta\mathbf{W} + (1-\theta)\mathbf{I}$ . Since  $\mu > 0$  and  $\theta \in [0, 1]$ ,  $\mathbf{H}$  and  $\mathbf{W}_\theta$  are symmetric with eigenvalues in  $[0, 1]$ . Moreover, it is clear that  $\|\mathbf{W}_\theta\|_2 \leq 1$  and  $\|\mathbf{H}\|_2 \leq 1$ . Also, since  $\text{fix}(\mathbf{W}_\theta) = \text{fix}(\mathbf{W})$  and  $\text{fix}(\mathbf{H}) = \ker(\mathbf{A})$ , we have

$$\text{fix}(\mathbf{W}_\theta) \cap \text{fix}(\mathbf{H}) = \{\mathbf{0}\}.$$

The rest of the proof is identical to that for  $\mathbf{P}_\gamma$ . □

**3.2. Linear convergence.** We now discuss the main result of the paper. The idea is to express Algorithm 3.1 and Algorithm 3.2 as a dynamical system in  $\mathbb{R}^{2n}$ . The transition operator is time-varying but is shown to converge to an operator with a spectral radius strictly less than 1.

THEOREM 3.5. *Let (2.1) be the loss in Algorithm 3.1 and Algorithm 3.2,  $\lim_{k \rightarrow \infty} \alpha_k = 1$ , and that  $\mathbf{W}$  and  $\mathbf{A}$  satisfy Assumption 2.1. Then the iterates of Algorithm 3.1 exhibit global linear convergence for any  $\gamma \in (0, 1/\lambda_{\max}(\mathbf{A}^\top\mathbf{A}))$ . On the other hand, the iterates of Algorithm 3.2 exhibit global linear convergence for any  $L \geq 1$ .*

*Proof.* The gradient of (2.1) is  $\nabla f(\mathbf{x}) = \mathbf{A}^\top(\mathbf{A}\mathbf{x} - \mathbf{b})$ . Therefore, we can write step 4 of Algorithm 3.1 as  $\mathbf{x}_k = \mathbf{P}_\gamma\mathbf{y}_k + \mathbf{q}$ , where  $\mathbf{P}_\gamma$  is defined in (3.4) and  $\mathbf{q} := \gamma\mathbf{W}\mathbf{A}^\top\mathbf{b}$ . Furthermore, from step 5, we have

$$(3.5) \quad \mathbf{x}_k = (1 + \alpha_k)\mathbf{P}_\gamma\mathbf{x}_{k-1} - \alpha_{k-1}\mathbf{P}\mathbf{x}_{k-2} + \mathbf{q}.$$

For  $k \geq 1$ , define the state space variables

$$(3.6) \quad \mathbf{z}_k = \begin{pmatrix} \mathbf{x}_k \\ \mathbf{x}_{k-1} \end{pmatrix} \in \mathbb{R}^{2n}.$$

<sup>1</sup>This part is similar to the proof of [1, Lemma 1]; however, the present argument is simpler as our assumption on the spectrum is weaker. Moreover, the analysis is necessary for the other operator  $\mathbf{P}_{\mu,\theta}$ .

Since  $\ker(\mathbf{A}) \cap \text{fix}(\mathbf{W}) = \{\mathbf{0}\}$  and  $\gamma \in (0, 1/\lambda_{\max}(\mathbf{A}^\top \mathbf{A}))$ , we know from Lemma 3.3 that  $\rho(\mathbf{P}_\gamma) < 1$ . In particular, this means  $\mathbf{I}_n - \mathbf{P}_\gamma$  is nonsingular, and we define

$$(3.7) \quad \mathbf{x}^* := (\mathbf{I}_n - \mathbf{P}_\gamma)^{-1} \mathbf{q}, \quad \mathbf{z}^* := \begin{pmatrix} \mathbf{x}^* \\ \mathbf{x}^* \end{pmatrix} \in \mathbb{R}^{2n}.$$

We now use Lemma 3.1 to show that  $\{\mathbf{z}_k\}_{k \geq 1}$  converges linearly to  $\mathbf{z}^*$ . From (3.5), we can write  $\mathbf{z}_k = \mathbf{T}_k(\mathbf{z}_{k-1})$ , where

$$\mathbf{R}_k := \begin{pmatrix} (1 + \alpha_k) \mathbf{P} & -\alpha_k \mathbf{P} \\ \mathbf{I}_n & \mathbf{0}_n \end{pmatrix}, \quad \mathbf{s} := \begin{pmatrix} \mathbf{q} \\ \mathbf{0} \end{pmatrix}, \quad \mathbf{T}_k(\mathbf{z}) := \mathbf{R}_k \mathbf{z} + \mathbf{s}.$$

The setup is now similar to Lemma 3.1. We define

$$\mathbf{R}_\infty := \begin{pmatrix} 2\mathbf{P}_\gamma & -\mathbf{P}_\gamma \\ \mathbf{I}_n & \mathbf{0}_n \end{pmatrix},$$

and verify the assumptions in Lemma 3.1. Since  $\alpha_k \rightarrow 1$ , it is evident that  $\lim_{k \rightarrow \infty} \mathbf{R}_k = \mathbf{R}_\infty$ . On the other hand, it follows from Lemma 3.3 that  $\sigma(\mathbf{P}_\gamma) \subset [0, 1)$ . Hence, from Proposition 3.2, we have  $\rho(\mathbf{R}_\infty) < 1$ . Finally, we can check from (3.7) that  $\mathbf{z}^* \in \text{fix}(\mathbf{T}_k)$  for all  $k \geq 1$ . Therefore, we can conclude from Lemma 3.1 that there exist  $\beta \in [0, 1)$ , constant  $C > 0$ , norm  $\|\cdot\|$  on  $\mathbb{R}^{2n}$ , and  $K \geq 1$  such that

$$(3.8) \quad \forall k \geq K : \quad \|\mathbf{z}_k - \mathbf{z}^*\| \leq C \beta^k.$$

Since  $\|\mathbf{x}_k - \mathbf{x}^*\| \leq c \|\mathbf{z}_k - \mathbf{z}^*\|$  for some constant  $c > 0$  (see definition (3.6)), it is immediate from (3.8) that  $\{\mathbf{x}_k\}_{k \geq 1}$  converges linearly to  $\mathbf{x}^*$ .

The analysis for Algorithm 3.2 is similar. For the loss in (2.1), we have

$$\text{prox}_{(\lambda L)^{-1} f}(\mathbf{y}) = \mathbf{H}_\mu \mathbf{y} + \mathbf{r},$$

where  $\mu := (\lambda L)^{-1}$ ,  $\mathbf{H}_\mu := (\mathbf{I}_n + \mu \mathbf{A}^\top \mathbf{A})^{-1}$ , and  $\mathbf{r} := \mu \mathbf{H}_\mu \mathbf{A}^\top \mathbf{b}$ . Thus, we can write step 4 of Algorithm 3.2 as  $\mathbf{x}_k = \mathbf{H}_\mu \mathbf{v}_{k-1} + \mathbf{r}$ . Combining this with steps 5 and 6, we have

$$\mathbf{x}_k = (1 + \alpha_{k-1}) \mathbf{P}_{\mu, \theta} \mathbf{x}_{k-1} - \alpha_{k-1} \mathbf{P}_{\mu, \theta} \mathbf{x}_{k-2} + \mathbf{r},$$

where

$$\mathbf{P}_{\mu, \theta} := \mathbf{H}_\mu \mathbf{W}_\theta \quad \text{and} \quad \mathbf{W}_\theta := \theta \mathbf{W} + (1 - \theta) \mathbf{I}_n.$$

Beyond this point, the analysis proceeds as before. Namely, we move from the iterates  $\{\mathbf{x}_k\}$  to the state space sequence  $\{\mathbf{z}_k\}$ , establish linear convergence of  $\{\mathbf{z}_k\}$  using Proposition 3.2 and Lemma 3.1, and finally deduce linear convergence of  $\{\mathbf{x}_k\}$ .  $\square$

**COROLLARY 3.6.** *Suppose PnP-FISTA or RED-APG is used for inpainting, deblurring, or superresolution, where the loss is (2.1) and the denoiser is (2.4). Then the iterates of PnP-FISTA (resp. RED-APG) converge globally and linearly to a unique reconstruction for any  $0 < \gamma < 1/\lambda_{\max}(\mathbf{A}^\top \mathbf{A})$  (resp.  $L \geq 1$ ).*

*Proof.* This follows from Theorem 3.5. Indeed, we have  $\alpha_k = (t_k - 1)/t_{k+1}$  for PnP-FISTA and RED-APG which converges to 1. Hence, we have  $\alpha_k \rightarrow 1$  for PnP-FISTA and RED-APG. The rest of the argument follows from Proposition 2.3 and Theorem 3.5.  $\square$

**3.3. Extension to nonsymmetric  $\mathbf{W}$ .** The convergence analysis for PnP-FISTA can be extended to the nonsymmetric kernel denoiser  $\mathbf{W}_{\text{NLM}}$  defined in (2.3). However, as pointed out in [10], we need to work with an inner product different from the standard inner product on  $\mathbb{R}^n$ . More precisely, we need to run PnP-FISTA in the Euclidean space



$(\mathbb{R}^n, \langle \cdot, \cdot \rangle_{\mathbf{D}})$ , where the inner-product  $\langle \cdot, \cdot \rangle_{\mathbf{D}}$  is given by<sup>2</sup>

$$(3.9) \quad \langle \mathbf{x}, \mathbf{y} \rangle_{\mathbf{D}} := \mathbf{x}^{\top} \mathbf{D} \mathbf{y}.$$

We note that (3.9) is a valid inner product since  $\mathbf{D}$  is positive definite by construction.

Accordingly, step 4 in PnP-FISTA (and Algorithm 3.1) must be changed to

$$(3.10) \quad \mathbf{x}_k = \mathbf{W}_{\text{NLM}}(\mathbf{y}_k - \gamma \nabla_{\mathbf{D}} f(\mathbf{y}_k)),$$

where  $\nabla_{\mathbf{D}} f$  is the gradient of  $f$  with respect to the inner-product (3.9). In fact, we have  $\nabla_{\mathbf{D}} f(\mathbf{y}) = \mathbf{D}^{-1} \mathbf{A}^{\top} (\mathbf{A} \mathbf{y} - \mathbf{b})$ . Hence, we can write (3.10) as

$$\mathbf{x}_k = \mathbf{W}_{\text{NLM}}(\mathbf{y}_k - \gamma \mathbf{D}^{-1} \mathbf{A}^{\top} (\mathbf{A} \mathbf{y}_k - \mathbf{b})) = \mathbf{P}_{\gamma} \mathbf{y}_k + \mathbf{q},$$

where

$$(3.11) \quad \mathbf{P}_{\gamma} := \mathbf{W}_{\text{NLM}}(\mathbf{I}_n - \gamma \mathbf{D}^{-1} \mathbf{A}^{\top} \mathbf{A}) \quad \text{and} \quad \mathbf{q} := \gamma \mathbf{W}_{\text{NLM}} \mathbf{D}^{-1} \mathbf{A}^{\top} \mathbf{b}.$$

The other updates in PnP-FISTA stay unchanged. Following [10], we will refer to this modified algorithm as `scaled-PnP-FISTA`. Similar to Corollary 3.6, we have the following result<sup>3</sup>.

**COROLLARY 3.7.** *Suppose we use `scaled-PnP-FISTA` for inpainting, deblurring, or superresolution, where the loss is (2.1) and the denoiser is (2.3). Then the iterates exhibit global linear convergence for any  $0 < \gamma < 1/\lambda_{\max}(\mathbf{D}^{-1/2} \mathbf{A}^{\top} \mathbf{A} \mathbf{D}^{-1/2})$ .*

We remark that since  $\mathbf{D}_{ii} \geq 1$ , we have  $\lambda_{\max}(\mathbf{D}^{-1/2} \mathbf{A}^{\top} \mathbf{A} \mathbf{D}^{-1/2}) \leq \lambda_{\max}(\mathbf{A}^{\top} \mathbf{A})$ . Thus, we can also use the interval  $(0, 1/\lambda_{\max}(\mathbf{A}^{\top} \mathbf{A}))$  in Corollary 3.7, which does not depend on  $\mathbf{D}$ .

*Proof.* We are done if we can show that  $\sigma(\mathbf{P}_{\gamma}) \subset [0, 1)$ , where  $\mathbf{P}_{\gamma}$  is as defined in (3.11). The rest of the analysis is identical to Corollary 3.6.

To verify  $\sigma(\mathbf{P}_{\gamma}) \subset [0, 1)$ , we use (2.3) to write  $\mathbf{P}_{\gamma} \sim \mathbf{D}^{\frac{1}{2}} \mathbf{P}_{\gamma} \mathbf{D}^{-\frac{1}{2}} = \mathbf{W}_s \mathbf{G}_{\gamma}$ , where

$$\mathbf{W}_s := \mathbf{D}^{-\frac{1}{2}} \mathbf{K} \mathbf{D}^{-\frac{1}{2}} \quad \text{and} \quad \mathbf{G}_{\gamma} := \mathbf{I}_n - \gamma \mathbf{D}^{-\frac{1}{2}} \mathbf{A}^{\top} \mathbf{A} \mathbf{D}^{-\frac{1}{2}}$$

In particular,  $\sigma(\mathbf{P}_{\gamma}) = \sigma(\mathbf{W}_s \mathbf{G}_{\gamma})$  and  $\mathbf{W}_s, \mathbf{G}_{\gamma} \in \mathbb{S}^n$ . We are now in the setup of Lemma 3.3. Since  $\mathbf{W}_s$  is similar to  $\mathbf{W}_{\text{NLM}}$  and  $\sigma(\mathbf{W}_{\text{NLM}}) \subset [0, 1]$  (Proposition 2.2), we have  $\sigma(\mathbf{W}_s) \subset [0, 1]$ . On the other hand, it is not difficult to verify that  $\sigma(\mathbf{G}_{\gamma}) \subset [0, 1]$  if  $0 < \gamma < 1/\lambda_{\max}(\mathbf{D}^{-1/2} \mathbf{A}^{\top} \mathbf{A} \mathbf{D}^{-1/2})$ . Furthermore,

$$\text{fix}(\mathbf{W}_s) \cap \text{fix}(\mathbf{G}_{\gamma}) = (\mathbf{D}^{\frac{1}{2}} \text{span}(\mathbf{1})) \cap (\mathbf{D}^{\frac{1}{2}} \ker(\mathbf{A})) = \{\mathbf{0}\},$$

since  $\text{fix}(\mathbf{W}_s) = \mathbf{D}^{\frac{1}{2}} \text{fix}(\mathbf{W}_{\text{NLM}})$  and  $\text{fix}(\mathbf{W}_{\text{NLM}}) = \text{span}(\mathbf{1})$  by Proposition 2.2. Similar to Lemma 3.3, we can now easily verify that  $\sigma(\mathbf{W}_s \mathbf{G}_{\gamma}) \subset [0, 1)$ .  $\square$

**4. Numerical results.** We present results<sup>4</sup> for inpainting, deblurring, and superresolution<sup>5</sup> to provide numerical evidence supporting the theoretical results. In particular, we validate the convergence theorems, confirm the uniqueness of the reconstruction for different initializations, and test whether  $\rho(\mathbf{R}_{\infty}) < 1$ .

For deblurring, we applied an isotropic Gaussian blur of  $25 \times 25$  size and standard deviation 1.6. Additionally, we introduced white Gaussian noise of standard deviation

<sup>2</sup>Note that  $\mathbf{W}_{\text{NLM}}$  is self-adjoint with respect to (3.9). Moreover, as observed in [10],  $\mathbf{W}_{\text{NLM}}$  can be expressed as the proximal operator (w.r.t. the norm induced by (3.9)) of a closed, proper, and convex function.

<sup>3</sup>A similar analysis holds for RED-APG, where we can establish linear convergence for a nonsymmetric kernel denoiser by incorporating (3.9) and the corresponding norm in Algorithm 3.2.

<sup>4</sup>The code is available here: <https://github.com/arghyasinha/PnP-FISTA>.

<sup>5</sup>The test images are from the Set12 database: <https://github.com/cszn/DnCNN/tree/master/testsets/Set12>

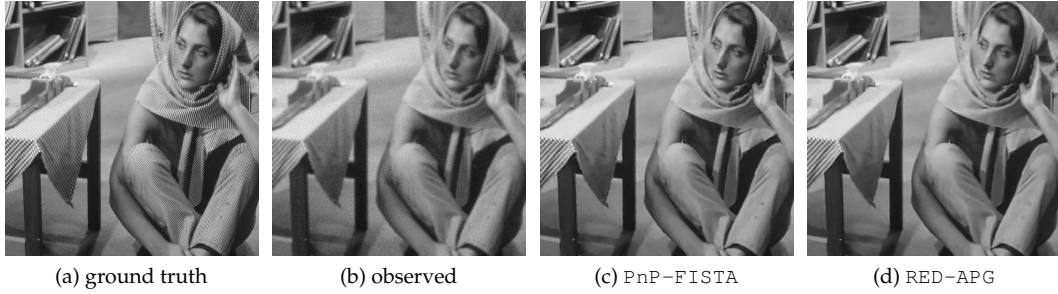


FIG. 2. Deblurring using a symmetric kernel denoiser. The PSNR and SSIM values are (b) 23.07, 0.5317, (c) 24.16, 0.7053, and (d) 24.15, 0.7025. We have used  $\gamma = 0.9$  for PnP-FISTA and  $\lambda = 1, L = 2$  for RED-APG and (b) observed image as the guide image for the denoiser.

TABLE 1  
Values of  $\rho(\mathbf{R}_\infty)$  for for different applications and parameter settings.

$\gamma, 1/L$	PnP-FISTA		RED-APG	
	Inpainting	Deblurring	Inpainting	Deblurring
0.10	0.993389	0.999920	0.996205	0.999914
0.25	0.992201	0.999907	0.997254	0.999905
0.50	0.991614	0.999893	0.994531	0.999893
0.75	0.991415	0.999884	0.991786	0.999884
0.90	0.991297	0.999880	0.990136	0.999880

$\sigma = 0.03$ . For inpainting, we randomly sampled 30% pixels. In all the experiments, we have used the symmetric DSG-NLM denoiser [34]. The deblurring and inpainting results are shown in Figure 2 and Figure 3. We demonstrate in Figure 3 that the PnP-FISTA iterates converge to the same reconstruction independent of the initialization (Theorem 3.5). The results for a  $2\times$ -superresolution experiment are shown in Figure 4, where we have compared the reconstruction from DSG-NLM with that obtained using trained denoisers such as DnCNN [39] and DRUNet [38]. We have used the Lipschitz-constrained DnCNN<sup>6</sup> denoiser from [29], which comes with a convergence guarantee for (1.3). The DRUNet result is superior to DnCNN [29] and DSG-NLM. However, we note that DRUNet does not come with convergence guarantees for PnP and RED (see Figure 1). While DnCNN achieves a higher PSNR than DSG-NLM, it introduces visual artifacts, possibly due to the low noise levels used during its training [29]. Overall, we observe a tradeoff between the regularization capacity of a denoiser and its convergence properties, a challenge that is widely recognized within the community [14, 18, 26, 36].

We next compute the spectral radius  $\rho(\mathbf{R}_\infty)$  using the power method [13]. We recall that  $\rho(\mathbf{R}_\infty)$  is a lower bound on the convergence rate  $\beta$  in (3.8). As shown in Table 1,  $\rho(\mathbf{R}_\infty)$  is very close to but strictly less than one for inpainting and deblurring (Proposition 3.2)

Finally, we study the empirical convergence of Algorithm 3.1 and Algorithm 3.2 for different choices of the momentum parameter  $\alpha_k$  (Theorem 3.5). This is done for the inpainting experiment in Figure 3. Along with the  $\{\alpha_k\}$  sequence in Beck [4] and Chambolle [7], we have used  $\alpha_k = 1 - 1/\log(k + 1)$  and  $\alpha_k = 1 - (0.5)^k$  that have the property  $\alpha_k \rightarrow 1$ . We plot the distance of the iterates from the unique limit point in Figure 5. Notably, observe that the iterates of Algorithm 3.1 can be slower to converge compared to the non-accelerated variants PnP-ISTA and RED-PG (Algorithm 3.1 and Algorithm 3.2), depending on the choice of  $\{\alpha_k\}$ . This is consistent with the findings in [28, 35].

<sup>6</sup><https://deepinv.github.io/deepinv/deepinv.denoisers.html#pretrained-weights>

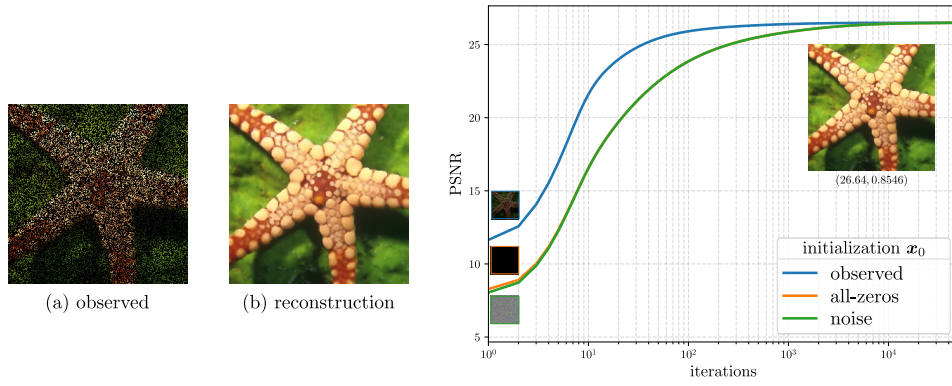


FIG. 3. Global convergence of  $PnP$ -FISTA. Inpainting results with different initialization  $\mathbf{x}_0$  (see the legend) converges to the same reconstruction (b) having PSNR 26.64 and SSIM 0.8546. We have used  $PnP$ -FISTA with  $\gamma = 0.9$ , and median filtered the observed image to get the guide image.

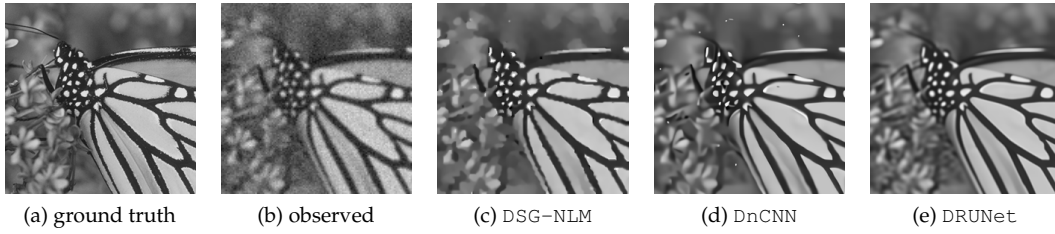


FIG. 4. Comparison of superresolution results with different denoisers. The forward operator is  $\mathbf{A} = \mathbf{S}\mathbf{B}$ , where  $\mathbf{B}$  is  $25 \times 25$  Gaussian blur with standard deviation 1.6 and  $\mathbf{S}$  is  $2 \times$ -downsampling. We also added white Gaussian noise of strength  $\sigma = 0.04$  to the measurement. The PSNR and SSIM values are (c) 25.27, 0.8201, (d) 25.35, 0.8324, and (e) 25.99, 0.8445. We used bicubic interpolation on the observed image to generate a guide image for DSG-NLM.

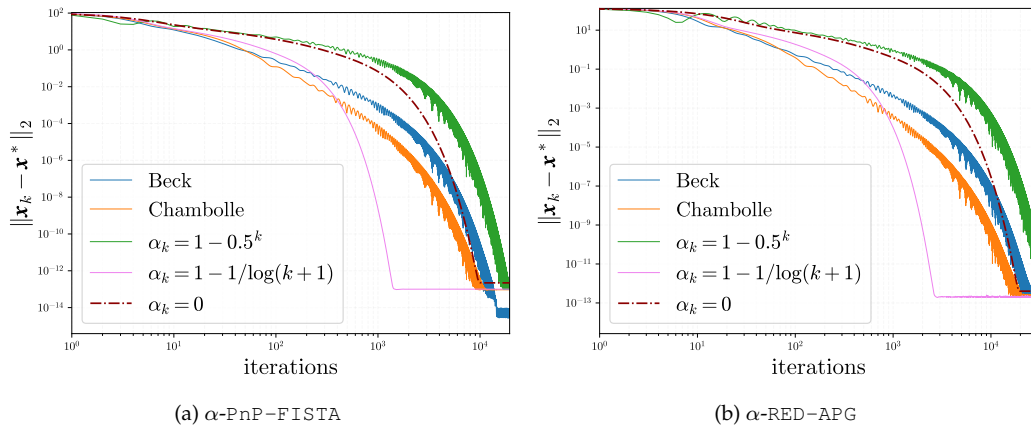


FIG. 5. Iterate convergence for different  $\{\alpha_k\}$  having the property  $\alpha_k \rightarrow 1$ . The case  $\alpha_k = 0$  correspond to  $PnP$ -ISTA and RED-PG, the non-accelerated variants of  $PnP$ -FISTA and RED-APG. The limit point  $\mathbf{x}^*$  was approximated using 20000 iterations of  $PnP$ -FISTA and 30000 iterations of RED-APG using the Beck sequence of  $\{\alpha_k\}$ . The parameters used are  $\gamma = 0.9$  for  $PnP$ -FISTA and  $\lambda = 1, L = 2$  for RED-APG.

**5. Conclusion.** We presented a concise analysis of the global linear convergence of FISTA in the context of regularizing linear inverse problems with symmetric denoisers. Additionally, we showed how the results can be extended to nonsymmetric denoisers by operating in an appropriate Euclidean space and using a scaled variant of the original algorithm. We restricted the scope to linear denoisers to keep the analysis tractable. However, data-driven linear denoisers are interesting in their own right in that they come with fast algorithms [24] and give good reconstructions for different applications. It would be interesting to see if the present analysis could shed some insights on the convergence theory of trained nonlinear denoisers that give state-of-the-art reconstructions.

## REFERENCES

- [1] C. D. ATHALYE, K. N. CHAUDHURY, AND B. KUMAR, *On the contractivity of plug-and-play operators*, IEEE Signal Process. Lett., 30 (2023), pp. 1447–1451.
- [2] H. BAUSCHKE AND P. COMBETTES, *Convex Analysis and Monotone Operator Theory in Hilbert Spaces*, New York: Springer, 2019.
- [3] A. BECK, *First-Order Methods in Optimization*, SIAM, 2017.
- [4] A. BECK AND M. TEOULLE, *A fast iterative shrinkage-thresholding algorithm for linear inverse problems*, SIAM J. Imaging Sci., 2 (2009), pp. 183–202.
- [5] C. A. BOUMAN, *Foundations of Computational Imaging: A Model-Based Approach*, SIAM, 2022.
- [6] A. BUADES, B. COLL, AND J. M. MOREL, *A non-local algorithm for image denoising*, Proc. CVPR, 2 (2005), pp. 60–65.
- [7] A. CHAMBOLLE AND CH. DOSSAL, *On the convergence of the iterates of the “fast iterative shrinkage/thresholding algorithm”*, J. Optim. Theory Appl., 166 (2015), pp. 968–982.
- [8] R. COHEN, M. ELAD, AND P. MILANFAR, *Regularization by denoising via fixed-point projection (RED-PRO)*, SIAM J. Imaging Sci., 14 (2021), pp. 1374–1406.
- [9] M. ELAD, B. KAWAR, AND G. VAKSMAN, *Image denoising: The deep learning revolution and beyond—a survey paper*, SIAM Journal on Imaging Sciences, 16 (2023), pp. 1594–1654.
- [10] R. G. GAVASKAR, C. D. ATHALYE, AND K. N. CHAUDHURY, *On plug-and-play regularization using linear denoisers*, IEEE Trans. Image Process., 30 (2021), pp. 4802–4813.
- [11] R. G. GAVASKAR, C. D. ATHALYE, AND K. N. CHAUDHURY, *On exact and robust recovery for plug-and-play compressed sensing*, Signal Processing, 211 (2023), p. 109100.
- [12] R. G. GAVASKAR AND K. N. CHAUDHURY, *Plug-and-play ISTA converges with kernel denoisers*, IEEE Signal Process. Lett., 27 (2020), pp. 610–614.
- [13] G. H. GOLUB AND C. F. V. LOAN, *Matrix Computations*, Johns Hopkins University Press, 1983.
- [14] A. GOJON, S. NEUMAYER, AND M. UNSER, *Learning weakly convex regularizers for convergent image-reconstruction algorithms*, SIAM J. Imaging Sci., 17 (2024), pp. 91–115.
- [15] A. HAUPTMANN, S. MUKHERJEE, C.-B. SCHÖNLIEB, AND F. SHERRY, *Convergent regularization in inverse problems and linear plug-and-play denoisers*, Foundations of Computational Mathematics, (2024).
- [16] J. HERTZSCH, S. NEUMAYER, AND G. STEIDL, *Convolutional proximal neural networks and plug-and-play algorithms*, Linear Algebra and its Applications, 631 (2021), pp. 203–234.
- [17] R. A. HORN AND C. R. JOHNSON, *Matrix Analysis*, Cambridge University Press, 2012.
- [18] S. HURAU, A. LECLAIRE, AND N. PAPADAKIS, *Gradient step denoiser for convergent plug-and-play*, Proc. ICLR, (2022).
- [19] P. R. JOHNSTONE AND P. MOULIN, *A Lyapunov analysis of FISTA with local linear convergence for sparse optimization*, arXiv preprint arXiv:1502.02281, (2015).
- [20] T. LIU, L. XING, AND Z. SUN, *Study on convergence of plug-and-play ISTA with adaptive-kernel denoisers*, IEEE Signal Process. Lett., 28 (2021), pp. 1918–1922.
- [21] D. A. LORENZ AND T. POCK, *An inertial forward-backward algorithm for monotone inclusions*, J. Math. Imaging Vis., 51 (2015), pp. 311–325.
- [22] P. MILANFAR, *A tour of modern image filtering: new insights and methods, both practical and theoretical*, IEEE Signal Process. Mag., 30 (2013), pp. 106–128.
- [23] P. MILANFAR, *Symmetrizing smoothing filters*, SIAM J. Imaging Sci., 6 (2013), pp. 263–284.
- [24] P. NAIR AND K. N. CHAUDHURY, *Fast high-dimensional kernel filtering*, IEEE Signal Process. Lett., 26 (2019), pp. 377–381.
- [25] P. NAIR AND K. N. CHAUDHURY, *Plug-and-play regularization using linear solvers*, IEEE Trans. Image Process., 31 (2022), pp. 6344–6355.
- [26] P. NAIR AND K. N. CHAUDHURY, *Averaged deep denoisers for image regularization*, J. Math. Imaging Vis., (2024), pp. 1–18.
- [27] P. NAIR, V. UNNI, AND K. N. CHAUDHURY, *Hyperspectral image fusion using fast high-dimensional denoising*, Proc. IEEE ICIP, (2019), pp. 3123–3127.
- [28] B. O’DONOGHUE AND E. CANDÈS, *Adaptive restart for accelerated gradient schemes*, Foundations of Computational Mathematics, 15 (2015), pp. 715–732.
- [29] J.-C. PESQUET, A. REPETTL, M. TERRIS, AND Y. WIAUX, *Learning maximally monotone operators for image recovery*, SIAM J. Imaging Sci., 14 (2021), pp. 1206–1237.

- [30] E. T. REEHORST AND P. SCHNITER, *Regularization by denoising: Clarifications and new interpretations*, IEEE Trans. Comput. Imag., 5 (2018), pp. 52–67.
- [31] Y. ROMANO, M. ELAD, AND P. MILANFAR, *The little engine that could: Regularization by denoising (RED)*, SIAM J. Imaging Sci., 10 (2017), pp. 1804–1844.
- [32] E. RYU, J. LIU, S. WANG, X. CHEN, Z. WANG, AND W. YIN, *Plug-and-play methods provably converge with properly trained denoisers*, Proc. ICML, (2019), pp. 5546–5557.
- [33] E. K. RYU, R. HANNAH, AND W. YIN, *Scaled relative graph: Nonexpansive operators via 2D euclidean geometry*, Mathematical Programming, 194 (2022), pp. 569–619.
- [34] S. SREEHARI, S. V. VENKATAKRISHNAN, B. WOHLBERG, G. T. BUZZARD, L. F. DRUMMY, J. P. SIMMONS, AND C. A. BOUMAN, *Plug-and-play priors for bright field electron tomography and sparse interpolation*, IEEE Trans. Comput. Imag., 2 (2016), pp. 408–423.
- [35] S. TAO, D. BOLEY, AND S. ZHANG, *Local linear convergence of ISTA and FISTA on the LASSO problem*, SIAM J. Optim., 26 (2016), pp. 313–336.
- [36] M. TERRIS, T. MOREAU, N. PUSTELNIK, AND J. TACHELLA, *Equivariant plug-and-play image reconstruction*, Proc. CVPR, (2024), pp. 25255–25264.
- [37] X. XU, Y. SUN, J. LIU, B. WOHLBERG, AND U. S. KAMILOV, *Provable convergence of plug-and-play priors with MMSE denoisers*, IEEE Signal Processing Letters, 27 (2020), pp. 1280–1284.
- [38] K. ZHANG, Y. LI, W. ZUO, L. ZHANG, L. VAN GOOL, AND R. TIMOFTE, *Plug-and-play image restoration with deep denoiser prior*, IEEE Trans. Pattern Anal. Mach. Intell., 44 (2021), pp. 6360–6376.
- [39] K. ZHANG, W. ZUO, Y. CHEN, D. MENG, AND L. ZHANG, *Beyond a Gaussian denoiser: Residual learning of deep cnn for image denoising*, IEEE Trans. on Image Process., 26 (2017), pp. 3142–3155.